ACS APPLIED MATERIALS & INTERFACES

Research Article

www.acsami.org

Porous Co_3O_4 Nanorods–Reduced Graphene Oxide with Intrinsic Peroxidase-Like Activity and Catalysis in the Degradation of Methylene Blue

Zhe Zhang, Jinhui Hao, Wenshu Yang, Baoping Lu, Xi Ke, Bailin Zhang, and Jilin Tang*

State Key Laboratory of Electroanalytical Chemistry, Changchun Institute of Applied Chemistry, Chinese Academy of Sciences, Changchun 130022, People's Republic of China, and University of Chinese Academy of Sciences, Beijing, 100049, People's Republic of China

Supporting Information

ABSTRACT: A facile two step process was developed for the synthesis of porous Co_3O_4 nanorods–reduced graphene oxide (PCNG) hybrid materials based on the hydrothermal treatment cobalt acetate tetrahydrate and graphene oxide in a glycerol–water mixed solvent, followed by annealing the intermediate of reduced graphene oxide-supported Co-$(CO_3)_{0.5}(OH)\cdot 0.11H_2O$ nanorods in a N_2 atmosphere. The morphology and microstructure of the composites were examined by X-ray diffraction, X-ray photoelectron spectroscopy, transmission electron microscopy and Raman spectroscopy. It is shown that the obtained PCNG have intrinsic peroxidase-like activity. The PCNG are utilized for the catalytic degradation of methylene blue. The good catalytic performance of the composites could be attributed to the synergy between the functions of porous Co_3O_4 nanorods and reduced graphene oxide.

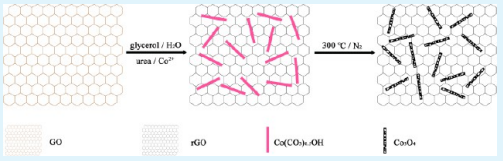

KEYWORDS: *graphene, nanorods, peroxidase-like activity, methylene blue*

1. INTRODUCTION

In recent years, porous metal oxides have attracted tremendous attention, because of their unique catalytic, electrochemical, magnetic, and adsorptive properties.[1−3] So far, porous materials can be prepared by two main approaches: soft template and hard template routes.[4−8] Soft templates include the self-assembly of surfactants, such as nonionic triblock copolymers. However, soft-template methods usually lead to amorphous frameworks.[9,10] Hard template methods use mesoporous silica or anodic alumina as sacrificial template, which require complex precedures.[11,12] Therefore, although challenging, the development of a template-free, low-cost, and environmentally benign approach for synthesis of porous metal oxide with unique and hierarchical structures is still of great importance. Recently, the thermal decomposition of hydroxide and carbonate has been proved to be an effective strategy for synthesizing porous metal oxide.[13−15] In this method, pores are formed when gases are released during the thermal decomposition of metallic salts. As an important transition-metal oxide, mixed-valency spinel cobalt oxide (Co_3O_4) has attracted enormous research interest, because of its applications in many fields, including gas sensors, catalysts, supercapacitor and lithium-ion batteries.[16−19] As the properties of Co_3O_4 strongly depend on their morphologies and structures, Co_3O_4 with various novel morphologies such as cubes,[20] rods,[21] wires,[22] tubes,[23] and sheets[24] have been synthesized.

Since its discovery in 2004,[25] graphene, which is a one-atom-thick, two-dimensional (2D), sp^2-bonded carbon material, has gained more and more attention, because of its fascinating properties such as giant electron mobility,[26] high thermal conductivity,[27] and extraordinary elasticity and stiffness.[28,29] It is providing tremendous new advances in various fields, such as field-effect transistors,[30] biological/chemical sensors,[31] energy storage and conversion devices,[32] and transparent conductors.[33] So far, several methods have been developed to produce graphene: (1) mechanical cleavage,[25] which can afford pristine perfect structured single-layer graphene; (2) epitaxial growth of graphene on a substrate;[34−36] (3) bottom-up fabrication;[37] and (4) chemically derived graphene from graphene oxide (GO).[38,39] Among these methods, because of the ease of preparation and processing, as well as the scalable production and low cost, chemically derived graphene hold the promise for integration into various hybrid architectures. Furthermore, GO have abundant oxygenate groups on their surface. These functional groups are assumed to be uniformly distributed on the GO surface, which allow GO can be easily dispersed in water, forming a monodispersed single-layer solution because of these oxygenate species. Based on these advantages of GO, various graphene-based hybrid materials by compositing graphene with other functional nanomaterials such as metal,[40−43] metal oxide,[44−50] and polymer[51−53] to attain synergistic effects lead to vast unprecedented possibilities.

Recently, various Co_3O_4-graphene hybrid materials have been synthesized. Dai's group reported a hybrid material consisting of Co_3O_4 nanocrystals grown on reduced graphene oxide (rGO) as a high-performance bifunctional catalyst for the

Received: February 3, 2013
Accepted: April 2, 2013
Published: April 2, 2013

   dx.doi.org/10.1021/am4004655 | ACS Appl. Mater. Interfaces 2013, 5, 3809−3815

Scheme 1. Illustration of the Procedure Used To Prepare PCNG

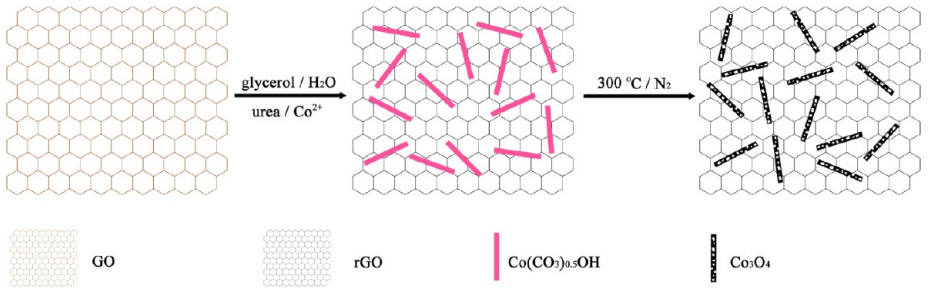

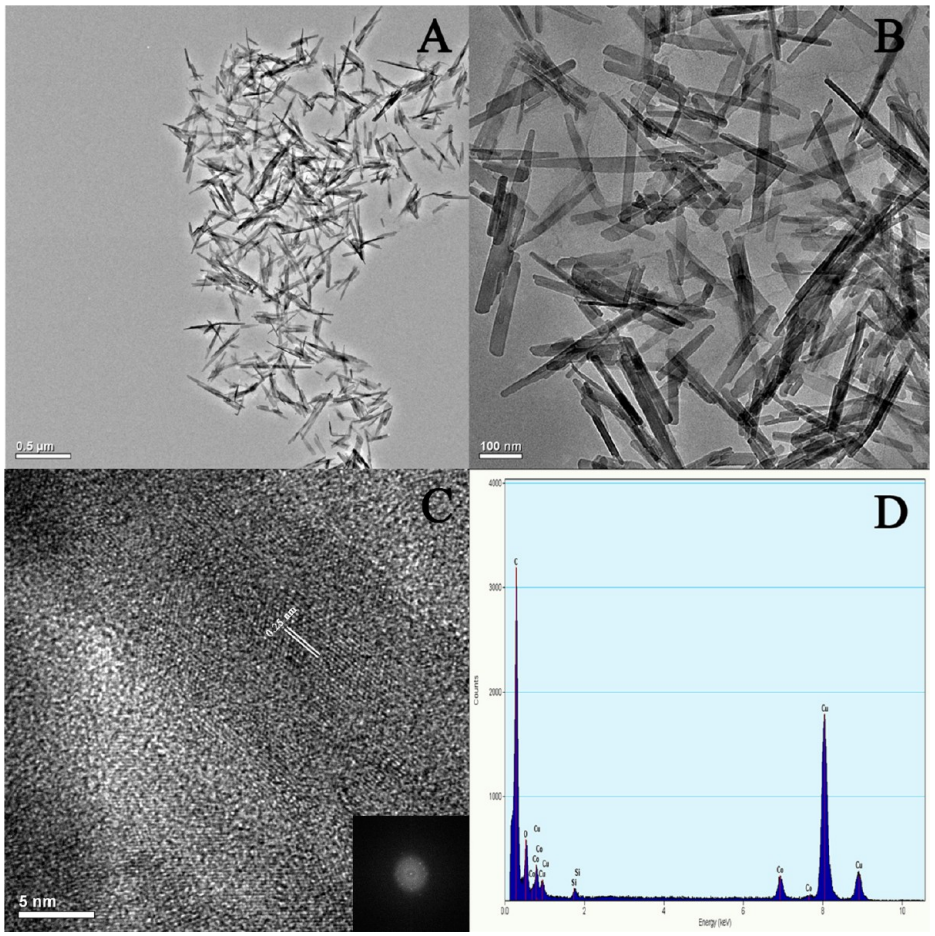

Figure 1. (A, B) Transmission electron microscopy (TEM) images of reduced graphene oxide-supported $Co(CO_3)_{0.5}(OH)\cdot 0.11H_2O$ nanorods at different magnifications. (C) High-resolution transmission electron microscopy (HRTEM) image of $Co(CO_3)_{0.5}(OH)\cdot 0.11H_2O$ nanorods. (D) EDX pattern of reduced graphene oxide-supported $Co(CO_3)_{0.5}(OH)\cdot 0.11H_2O$ nanorods.

oxygen reduction reaction (ORR) and oxygen evolution reaction (OER).[54] Qian et al. synthesized Co_3O_4 nanorods/graphene nanocomposites via a one-step solvothermal method.[55] Feng et al. described a novel strategy for the fabrication of graphene-encapsulated metal oxide by coassembly between negatively charged GO and positively charged oxide nanoparticles.[56] Herein, we report a facile strategy to synthesize porous Co_3O_4 nanorods-reduced graphene oxide (PCNG) hybrid materials by a two-step method. In the first step, cobalt carbonate hydroxide ($Co(CO_3)_{0.5}(OH)\cdot 0.11H_2O$) nanorods were grown on GO by hydrothermal treatment cobalt acetate tetrahydrate and GO in a glycerol–water mixed solvent. Subsequently, the intermediate was washed repeatedly with water and ethanol and annealed at 300 °C for 1 h in flowing nitrogen, which led to porosity of Co_3O_4 and further reduction of GO to form the PCNG hybrid. The obtained PCNG exhibited intrinsic peroxidase-like activity. When the as-prepared PCNG were applied for the catalytic oxidation of methylene blue (MB), they delivered high catalytic activity.

2. EXPERIMENTAL SECTION

2.1. Chemicals. Graphite was purchased from Alfa Aesar (325 mesh). Cobalt acetate tetrahydrate, glycerol, and urea were purchased from Beijing Chemical Reagent Factory. Other reagents were of analytical grade and were used as received without further purification. All aqueous solutions were prepared with Milli-Q water (18.2 MΩ cm).

2.2. Apparatus. UV–vis detection was carried out on a Cary 500 UV–vis-NIR spectrophotometer (Varian, Palo Alto, CA, USA).

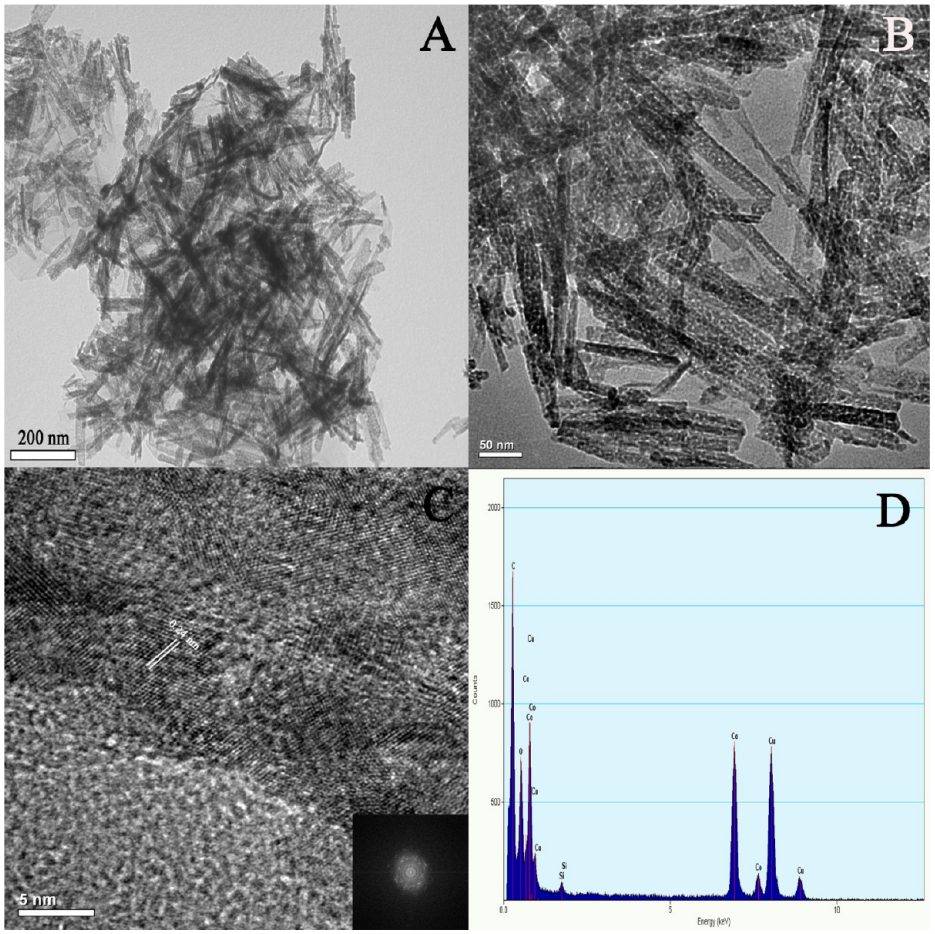

Figure 2. (A, B) TEM images of PCNG at different magnifications. (C) HRTEM image of Co_3O_4 nanorods. (D) EDX pattern of PCNG.

Raman spectra were acquired on a Renishaw (Renishaw, U.K.) 2000 model confocal microscopy Raman spectrometer with 514.5-nm wavelength incident laser light. X-ray photoelectron spectroscopy (XPS) measurement was performed on an ESCALAB-MKII spectrometer (VG Co., U.K.) with Al Kα X-ray radiation as the X-ray source for excitation. The sample for XPS characterization was deposited onto a Si slide. X-ray diffraction (XRD) spectra were obtained using a D8 ADVANCE system (Bruker, Germany) using Cu Kα (1.5406 Å) radiation. Transmission electron microscopy (TEM) and high-resolution transmission electron microscopy (HRTEM) images were obtained with a TECNAI G2 HRTEM system (Holland) with an accelerating voltage of 200 kV and a Hitachi Model H600 electron microscope (Japan) with an accelerating voltage of 100 kV. The sample for TEM characterization was prepared by placing a drop of prepared solution onto a carbon-coated copper grid and drying at room temperature. Thermogravimetric analysis (TGA) of sample was performed on a Pyris Diamond TG/DTA thermogravimetric analyzer (Perkin–Elmer Thermal Analysis). Sample was heated under an air atmosphere from room temperature to 900 °C at 10 °C/min.

2.3. Preparation of Graphene Oxide (GO). The graphite oxide was synthesized from graphite according to the literature.[20] Then, exfoliation of graphite oxide into graphene oxide (GO) was achieved by sonication of the dispersion for 60 min (80 W, 90% amplitude). The obtained brown dispersion was then subjected to centrifugation at 3000 rpm for 30 min with a rotor radius of 8 cm in order to remove any unexfoliated graphite oxide. Finally, a homogeneous aqueous GO solution (~0.5 mg/mL) was obtained.

2.4. Synthesis of PCNG. In the first step of preparing the PCNG, 1 mL of the GO dispersion (~5 mg/mL) was dispersed into a mixed solution of 12 mL of H_2O and 4 g of glycerol by sonication for 60 min. Subsequently, 0.1 g of urea and 60 mg of cobalt acetate tetrahydrate were added to the solution. After stirring for 30 min, the reaction solution was then transferred to a 40-mL Teflon-lined stainless steel autoclave and kept in an electric oven at 170 °C for 10 h. The autoclave was then taken out from the oven and left to cool to room temperature. The precipitate was collected via centrifugation, washed thoroughly with water and ethanol, and dried at 60 °C overnight. In the second step, the as-prepared intermediate was further treated at 300 °C in nitrogen for 1 h, using a heating rate of 3 °C min^{-1} to obtain the PCNG. Four exemplary composites were synthesized using different amounts of cobalt acetate tetrahydrate, denoted as PCNG-*X*, where *X* corresponds to the amount of cobalt acetate tetrahydrate (in milligrams). For comparison, the porous Co_3O_4 nanowires (PCN) were synthesized using the same procedure, but without the addition of GO.

2.5. Catalytic Oxidation Reaction. The catalysis experiment was carried out in a 100-mL glass flask that contained an aqueous MB solution (50 mg L^{-1}, 20 mL), and PCNG (1 mg). After a 30 wt % H_2O_2 solution (10 mL) was added, the mixture was heated to 80 °C with continuous stirring. At given time intervals, 0.5 mL of the mixture was removed and quickly diluted with distilled water to a total volume of 5 mL prior to analysis.

3. RESULTS AND DISCUSSION

The entire preparation strategy for constructing the PCNG is shown in Scheme 1 (for detailed experimental steps, please see the Experimental Section). In the first step, GO solution is mixed with a cobalt acetate solution, and Co^{2+} is selectively bonded with oxygenate groups through electrostatic attraction. After hydrothermal treatment in a glycerol–water mixed solvent, $Co(CO_3)_{0.5}(OH)\cdot 0.11H_2O$ nanorods are tightly bonded to the GO layer by the oxygenate groups, during

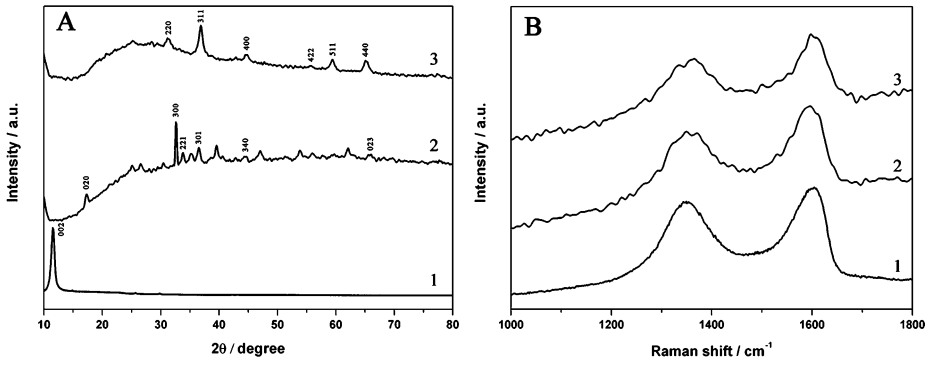

Figure 3. (A) XRD patterns and (B) Raman spectra of graphite oxide (spectrum 1), reduced graphene oxide-supported $Co(CO_3)_{0.5}(OH)\cdot 0.11H_2O$ nanorods (spectrum 2), and PCNG (spectrum 3).

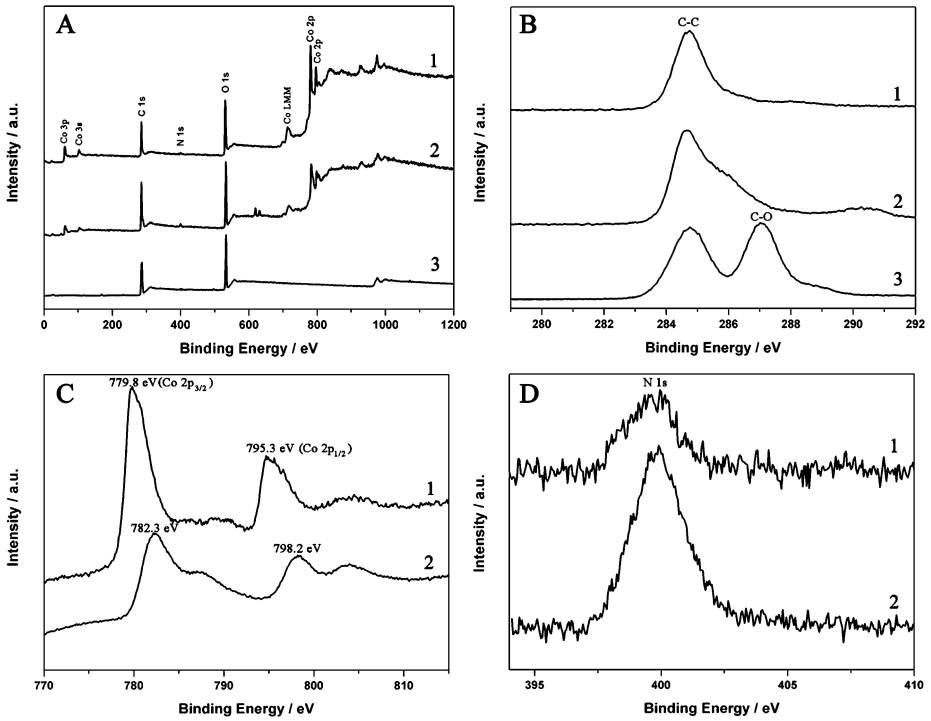

Figure 4. (A) XPS survey, (B) C 1s XPS spectra, (C) Co 2P XPS spectra, and (D) N 1s XPS spectra of PCNG (spectrum 1), reduced graphene oxide-supported $Co(CO_3)_{0.5}(OH)\cdot 0.11H_2O$ nanorods (spectrum 2), and graphite oxide (spectrum 3).

which GO was reduced into reduced graphene oxide as well. In the second step, the obtained intermediate (reduced graphene oxide-supported $Co(CO_3)_{0.5}(OH)\cdot 0.11H_2O$ nanorods) were converted to PCNG by treating at 300 °C for 1 h in a nitrogen atmosphere. Figure 1 is the representative TEM images of as-synthesized reduced graphene oxide-supported $Co(CO_3)_{0.5}(OH)\cdot 0.11H_2O$ nanorods at different magnifications. It can be clearly seen from Figure 1A that the GO sheets have been exfoliated and decorated randomly with the $Co(CO_3)_{0.5}(OH)\cdot 0.11H_2O$ nanorods. In the case of this hybrid, because of the interaction between the hydrophilic functional groups (e.g., −OH, −COOH) on GO and the hydroxyl groups on $Co(CO_3)_{0.5}(OH)\cdot 0.11H_2O$ nanorods, the $Co(CO_3)_{0.5}(OH)\cdot 0.11H_2O$ nanorods are well-dispersed on the reduced graphene oxide sheets. An enlarged TEM image (Figure 1B) shows that the diameters of the individual nanorods were in the range of 10−50 nm, and their length was 100−500 nm with a relatively smooth surface. Figure 1C shows a HRTEM image taken from the $Co(CO_3)_{0.5}(OH)\cdot 0.11H_2O$ nanorods, which indicates a lattice spacing of 0.24 nm and is quasi-single-crystalline in nature. Figure 1D shows the corresponding energy-dispersive X-ray (EDX) image, the results further confirm the presence of Co elements on the hybrid. In addition, as shown in Figure S1 in the Supporting Information, the density of the $Co(CO_3)_{0.5}(OH)\cdot 0.11H_2O$ nanorods on the surface of reduced graphene oxide can be easily changed by changing the weight ratio between GO and cobalt acetate tetrahydrate.

Reduced graphene oxide-supported $Co(CO_3)_{0.5}(OH)\cdot 0.11H_2O$ nanorods were annealed at 300 °C for 1 h in the nitrogen. The sintering temperature was selected due to the fact that $Co(CO_3)_{0.5}(OH)\cdot 0.11H_2O$ nanorods may decompose when the temperature rises above 300 °C. The morphology of the calcined product (PCNG) is further studied by TEM. As shown in the TEM images of PCNG at different magnifications (Figures 2A and 2B), the rodlike structure can be retained relatively well, although the nanorods have some aggregation. Under a higher magnification (Figure 2B), the

dx.doi.org/10.1021/am4004655 | ACS Appl. Mater. Interfaces 2013, 5, 3809−3815

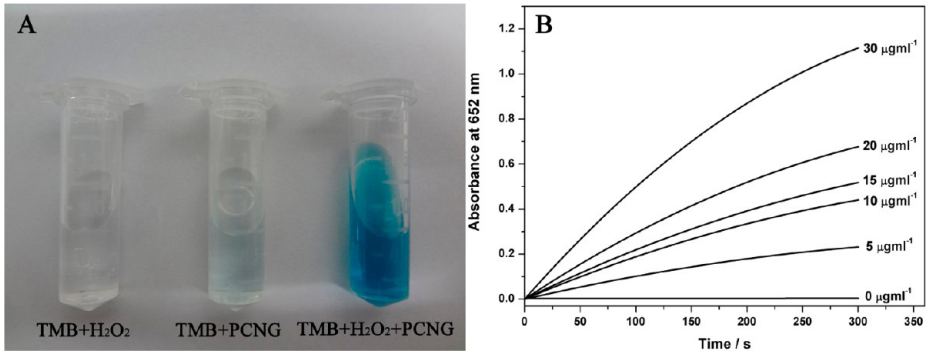

Figure 5. (A) Typical photographs of 1 mL of 0.5 mM TMB reaction solutions oxidized by PCNG-60 in the presence of H_2O_2 when incubated at room temperature in a pH 6.0 acetate buffer: (left) 50 mM H_2O_2 and 0.5 mM TMB; (middle) 30 μg mL^{-1} PCNG-60 and 0.5 mM TMB; and (right) 50 mM H_2O_2, 0.5 mM TMB, and 30 μg mL^{-1} PCNG-60. (B) Time-dependent absorbance changes at 652 nm in the absence or presence of different concentrations of PCNG-60 in buffer (100 mM acetate buffer, pH 6.0) at room temperature.

nanorods appear to be highly porous and composed of densely packed nanoparticles. Such a porous 1D structure is expected to facilitate liquid or gas to access and diffuse into the particles. The formation of pores may be attributed to the evolution of gas during the thermal decomposition reaction from Co$(CO_3)_{0.5}(OH)\cdot 0.11H_2O$ nanorods. The N_2 adsorption−desorption isotherm of the PCNG is depicted in Figure S5 in the Supporting Information, and the samples have a high surface area of 88 m^2 g^{-1} and a total pore volume of 0.42 cm^3 g^{-1}. The HRTEM image of an individual Co_3O_4 nanorod is shown in Figure 2C, which clearly reveals the polycrystalline nature of the Co_3O_4 nanorods. The lattice spacing of Co_3O_4 nanorods is 0.24 nm, corresponding to the (311) crystal planes of spinel Co_3O_4, which is in good agreement with the original XRD pattern in Figure 3A. TGA of the PCNG, as shown in Figure S2 in the Supporting Information, further illustrates that the Co_3O_4 nanorod content increases from 73.70% to 81.72% as the weight ratio between cobalt acetate tetrahydrate and GO increases. The crystal phase of the as-synthesized reduced graphene oxide-supported Co$(CO_3)_{0.5}(OH)\cdot 0.11H_2O$ nanorods and PCNG are determined by XRD (Figure 3A). Compared with the graphite oxide (Figure 3A, trace 1), the XRD pattern of the reduced graphene oxide-supported Co$(CO_3)_{0.5}(OH)\cdot 0.11H_2O$ nanorods (Figure 3A, trace 2) shows identified diffraction peaks from the pure orthorhombic Co$(CO_3)_{0.5}(OH)\cdot 0.11H_2O$ (JCPDS File Card No. 48-0083), revealing the crystalline nature of the Co$(CO_3)_{0.5}(OH)\cdot 0.11H_2O$ nanorods. The absence of peaks due to other phases indicates the high purity of the as-synthesized material. The XRD pattern (Figure 3A, trace 3) confirms that the heat-treated sample only contains pure cubic phase Co_3O_4 (JCPDS File Card No. 42-1467). This indicates the complete transformation of Co$(CO_3)_{0.5}(OH)\cdot 0.11H_2O$ into the Co_3O_4 phase. Raman spectroscopy is a useful nondestructive tool to distinguish ordered and disordered carbon structures. The presence of reduced graphene oxide in the hybrid is further confirmed by Raman spectroscopy. The Raman spectrum (Figure 3B, trace 1) of graphite oxide displays two prominent peaks at ca. 1349 and 1601 cm^{-1}, corresponding to the well-documented D and G bands, respectively. While for reduced graphene oxide-supported Co$(CO_3)_{0.5}(OH)\cdot 0.11H_2O$ nanorods (Figure 3B, trace 2) and PCNG (Figure 3B, trace 3), it is found that the intensity ratio of D/G shows a decreased value, compared to that of graphite oxide. This change suggests an increase in the average size of the crystalline graphene domains in the products. It is also found that the G band of the products have a red-shift compared to graphite oxide, which is attributed to the recovery of the hexagonal network of C atoms. Further evidence for the formation of the reduced graphene oxide-supported Co$(CO_3)_{0.5}(OH)\cdot 0.11H_2O$ nanorods and PCNG composite was obtained from XPS analysis. The XPS survey of PCNG (Figure 4A, trace 1) and reduced graphene oxide-supported Co$(CO_3)_{0.5}(OH)\cdot 0.11H_2O$ nanorods (Figure 4A, trace 2) revealed new Co 2p peaks, compared to the spectra of graphite oxide (Figure 4A, trace 3), which indicated the formation of Co_3O_4 and Co$(CO_3)_{0.5}(OH)\cdot 0.11H_2O$ on composite, respectively. XPS was also employed to further confirm the reduction of GO. Figure 4B shows the C 1s peaks, the peak intensities of oxygen-containing functionalities in the reduced graphene oxide-supported Co$(CO_3)_{0.5}(OH)\cdot 0.11H_2O$ nanorods (Figure 4B, trace 2) are much smaller than that in graphite oxide (Figure 4B, trace 3). These observations indicate considerable deoxygenation through the hydrothermal treatment process. While a nearly identical amount of oxygen-containing functionalities could be obtained in the PCNG (Figure 4B, trace 1), the subsequent thermal annealing resulted in a dramatic decrease in the oxygen-containing functional groups of GO. For the Co_3O_4 nanorods in Figure 4C, the Co 2p spectrum shows two major peaks with binding energy values at 779.8 and 795.2 eV, assigned to the Co $2p_{3/2}$ and Co $2p_{1/2}$ peaks, respectively, with a spin−orbit splitting of 15.4 eV. The absence of prominent shakeup satellite peaks in the Co 2p spectra further suggests the formation of the Co_3O_4 phase. Furthermore, XPS revealed nitrogen in PCNG (Figure 4D, trace 1) and reduced graphene oxide-supported Co$(CO_3)_{0.5}(OH)\cdot 0.11H_2O$ nanorods (Figure 4D, trace 2). The N-dopants were formed on reduced graphene oxide sheets via hydrothermal reactions between functional groups on GO and NH_4OH (provided by the slow hydrolysis of urea) in the solution. The overall nitrogen content of the PCNG evidently decreases, compared to reduced graphene oxide-supported Co$(CO_3)_{0.5}(OH)\cdot 0.11H_2O$ nanorods, after thermal annealing.

Peroxidase activity has a wide range of practical applications. For example, the ability to catalyze the oxidation of organic substrates to reduce their toxicity and/or to produce a color change is frequently used in wastewater treatment or as a detection tool.[57] Herein, PCNG is shown to possess intrinsic peroxidase-like activity that can catalyze the reaction of peroxidase substrate 3,3,5,5-tetramethylbenzidine (TMB) in the presence of H_2O_2. As shown in Figure 5A, upon the

addition of H_2O_2 and peroxidase substrate TMB, PCNG can produce a blue color reaction, indicating that PCNG has peroxidase-like catalytic activity. The maximum absorbance of the reaction mixture is 652 nm, which originates from the oxidation of TMB. Additional control experiments using TMB in the absence of PCNG or H_2O_2 show no oxidative reaction, which indicates that both the components are required for the reaction, as is also the case for horseradish peroxidase (HRP). Figure 5B shows the time-dependent absorbance changes (monitoring TMB absorbance change at 652 nm) against different concentrations of PCNG used, and it can be observed that the TMB oxidation rate catalyzed by the PCNG is dependent on the concentration of PCNG. The catalytic activity of the PCNG, similar to HRP, is dependent on pH and the H_2O_2 concentration. We measured the peroxidase-like activity of PCNG, while varying the pH from 1 to 12 and varying the temperature from 22 °C to 80 °C, and compared the results with the activity found in HRP over the same range of parameters (see Figure S3 in the Supporting Information). Under our experimental conditions, the optimal pH and H_2O_2 concentration for PCNG are pH 6.0 and 200 mM, respectively. More importantly, PCNG shows improved thermal stability. The HRP started to lose its activity above 40 °C, while the PCNG remained stable up to 60 °C. As shown in Figure S3C in the Supporting Information, the PCNG maintains 80% of its initial activity, even after 2 h of incubation at 80 °C, while the HRP loses all its initial activity. The stability in the presence of organic solvent was also performed. The HRP and PCNG were exposed to an aqueous solution containing 15% ethanol, THF, and DMF at room temperature for 12 h. As shown in Figure S3D in the Supporting Information, the PCNG maintains high activity while the free HRP loses almost all initial activity.

Rapid industrialization has led to an increased amount of discharged wastewater containing pollutant, which has detrimental effects on the environment and human health. The PCNG were used as a catalyst for wastewater treatment. MB, as a typical industrial pollutant, was chosen as a model to examine the catalytic performance of the PCNG. The degradation efficiency of the MB molecules was calculated by $(I_0 - I)/I_0$ (where I_0 is the absorbance at 665 nm at $t = 0$ and I is the absorbance at the same wavelength at a given reaction time). The degradation efficiency of the PCNG was 97% after 25 min (Figure 6), which was more effective than the pure Co_3O_4 nanorods or GO only. However, no obvious decolorization was observed without PCNG or H_2O_2 under the same conditions. The above results indicate that the PCNG could fulfill the electron transfer between MB and H_2O_2 in the oxidation of MB catalyzed by PCNG.[58] The enhanced catalytic activity of PCNG is due to the synergistic effect between Co_3O_4 nanorods and reduced graphene oxide. In this process, MB is more easily absorbed on the surface of the PCNG, due to the $\pi-\pi$ stacking between MB and aromatic regions of the reduced graphene oxide, and donates electrons from MB to the PCNG, which results in an increase in electron density and mobility in the PCNG. This would accelerate the transfer of electrons from the PCNG to H_2O_2, thus increasing the reaction rate of MB oxidation by H_2O_2.[58]

4. CONCLUSION

We present a facile two-step method to prepare porous Co_3O_4 nanorods–reduced graphene oxide (PCNG) hybrid materials using reduced graphene oxide-supported $Co(CO_3)_{0.5}(OH)\cdot 0.11H_2O$ nanorods as a intermediate and subsequent thermal treatment to form porous Co_3O_4 nanorods on the surface of reduced graphene oxide. It is shown that the obtained PCNG has intrinsic peroxidase-like activity and shows high thermal stability and against organic solvent. In addition, the obtained PCNG has good catalytic performance with regard to the degradation of MB.

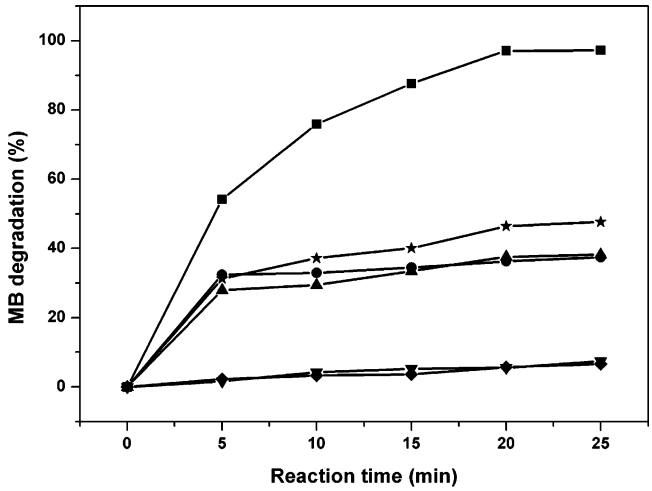

Figure 6. Dependence of time on MB degradation: (▼) PCNG + MB, (□) H_2O_2 + MB, (●) PCN + H_2O_2 + MB, (▲) GO + H_2O_2 + MB, (★) reduced graphene oxide-supported $Co(CO_3)_{0.5}(OH)\cdot 0.11H_2O$ nanorods + H_2O_2 + MB, and (■) PCN + H_2O_2 + MB.

■ ASSOCIATED CONTENT

Ⓢ Supporting Information

TEM images of reduced graphene oxide-supported $Co(CO_3)_{0.5}(OH)\cdot 0.11H_2O$ nanorods prepared at different amount of cobalt acetate tetrahydrate; TGA curves of PCNG; the peroxidase-like activity of the PCNG; TEM images of $Co(CO_3)_{0.5}(OH)\cdot 0.11H_2O$ nanorods and Co_3O_4 nanorods; nitrogen adsorption–desorption isotherms and pore-size distribution plots of PCNG; UV–vis spectrum of MB molecules. This material is available free of charge via the Internet at http://pubs.acs.org/.

■ AUTHOR INFORMATION

Corresponding Author

*Tel./Fax: +86 431-85262734. E-mail address: jltang@ciac.jl.cn.

Notes

The authors declare no competing financial interest.

■ ACKNOWLEDGMENTS

This work was supported by the National Basic Research Program of China (973 Program, No. 2011CB935800).

■ REFERENCES

(1) Wang, Y.; Zeng, H. C.; Lee, J. Y. *Adv. Mater.* **2006**, *18*, 645–649.
(2) Liu, H. S.; Bi, Z. H.; Sun, X. G.; Unocic, R. R.; Paranthaman, M. P.; Dai, S.; Brown, G. M. *Adv. Mater.* **2011**, *23*, 3450–3454.
(3) Chang, J.; Sun, J.; Xu, C. H.; Xu, H.; Gao, L. *Nanoscale* **2012**, *4*, 6786–6791.
(4) Tang, Z. Y.; Podsiadlo, P.; Shim, B. S.; Lee, J.; Kotov, N. A. *Adv. Funct. Mater.* **2008**, *18*, 3801–3808.
(5) Liu, L.; Fu, L.; Liu, Y.; Liu, Y. L.; Jiang, P.; Liu, S. Q.; Gao, M. Y.; Tang, Z. Y. *Cryst. Growth Des.* **2009**, *9*, 4793–4796.

(6) Yin, H. J.; Tang, H. J.; Wang, D.; Gao, Y.; Tang, Z. Y. *ACS Nano* **2012**, *6*, 8288−8297.
(7) Gao, Y.; Tang, Z. Y. *Small* **2011**, *7*, 2133−2146.
(8) Xiong, Y. S.; Tang, Z. Y. *Sci. China Chem.* **2012**, *55*, 2272−2282.
(9) Meng, Y.; Gu, D.; Zhang, F. Q.; Shi, Y. F.; Yang, H. F.; Li, Z.; Yu, C. Z.; Tu, B.; Zhao, D. Y. *Angew. Chem., Int. Ed.* **2005**, *44*, 7053−7059.
(10) Brezesinski, T.; Wang, J.; Tolbert, S. H.; Dunn, B. *Nat. Mater.* **2010**, *9*, 146−151.
(11) Liu, R.; Wu, D.; Feng, X.; Muellen, K. *Angew. Chem., Int. Ed.* **2010**, *49*, 2565−2569.
(12) Wang, Y.; Lee, J. Y.; Zeng, H. C. *Chem. Mater.* **2005**, *17*, 3899−3903.
(13) Bai, Z.; Sun, B.; Fan, N.; Ju, Z.; Li, M.; Xu, L.; Qian, Y. *Chem.−Eur. J.* **2012**, *18*, 5319−5324.
(14) Wang, B.; Zhu, T.; Wu, H. B.; Xu, R.; Chen, J. S.; Lou, X. W. *Nanoscale* **2012**, *4*, 2145−2149.
(15) Yuan, C.; Li, J.; Hou, L.; Zhang, X.; Shen, L.; Lou, X. W. *Adv. Funct. Mater.* **2012**, *22*, 4592−4597.
(16) Xiao, X.; Liu, X.; Zhao, H.; Chen, D.; Liu, F.; Xiang, J.; Hu, Z.; Li, Y. *Adv. Mater.* **2012**, *24*, 5762−5766.
(17) Rakhi, R. B.; Chen, W.; Cha, D.; Alshareef, H. N. *Nano Lett.* **2012**, *12*, 2559−2567.
(18) Xie, X.; Li, Y.; Liu, Z.-Q.; Haruta, M.; Shen, W. *Nature* **2009**, *458*, 746−749.
(19) Sun, C.; Rajasekhara, S.; Chen, Y.; Goodenough, J. B. *Chem. Commun.* **2011**, *47*, 12852−12854.
(20) Hu, L.; Peng, Q.; Li, Y. *J. Am. Chem. Soc.* **2008**, *130*, 16136−16137.
(21) Mei, W.; Huang, J.; Zhu, L.; Ye, Z.; Mai, Y.; Tu, J. *J. Mater. Chem.* **2012**, *22*, 9315−9321.
(22) Liu, J.; Jiang, J.; Cheng, C.; Li, H.; Zhang, J.; Gong, H.; Fan, H. J. *Adv. Mater.* **2011**, *23*, 2076−2081.
(23) Lou, X. W.; Deng, D.; Lee, J. Y.; Feng, J.; Archer, L. A. *Adv. Mater.* **2008**, *20*, 258−262.
(24) Liang, H.; Raitano, J. M.; Zhang, L.; Chan, S.-W. *Chem. Commun.* **2009**, *45*, 7569−7571.
(25) Novoselov, K. S.; Geim, A. K.; Morozov, S. V.; Jiang, D.; Zhang, Y.; Dubonos, S. V.; Grigorieva, I. V.; Firsov, A. A. *Science* **2004**, *306*, 666−669.
(26) Balandin, A. A.; Ghosh, S.; Bao, W.; Calizo, I.; Teweldebrhan, D.; Miao, F.; Lau, C. N. *Nano Lett.* **2008**, *8*, 902−907.
(27) Geim, A. K.; Novoselov, K. S. *Nat. Mater.* **2007**, *6*, 183−191.
(28) Lee, C.; Wei, X.; Kysar, J. W.; Hone, J. *Science* **2008**, *321*, 385−388.
(29) Bunch, J. S.; Verbridge, S. S.; Alden, J. S.; van der Zande, A. M.; Parpia, J. M.; Craighead, H. G.; McEuen, P. L. *Nano Lett.* **2008**, *8*, 2458−2462.
(30) Ohno, Y.; Maehashi, K.; Matsumoto, K. *J. Am. Chem. Soc.* **2010**, *132*, 18012−18013.
(31) He, S. J.; Song, B.; Li, D.; Zhu, C. F.; Qi, W. P.; Wen, Y. Q.; Wang, L. H.; Song, S. P.; Fang, H. P.; Fan, C. H. *Adv. Funct. Mater.* **2010**, *20*, 453−459.
(32) Paek, S. M.; Yoo, E.; Honma, I. *Nano Lett.* **2009**, *9*, 72−75.
(33) Wang, X.; Zhi, L. J.; Mullen, K. *Nano Lett.* **2008**, *8*, 323−327.
(34) Emtsev, K. V.; Bostwick, A.; Horn, K.; Jobst, J.; Kellogg, G. L.; Ley, L.; McChesney, J. L.; Ohta, T.; Reshanov, S. A.; Roehrl, J.; Rotenberg, E.; Schmid, A. K.; Waldmann, D.; Weber, H. B.; Seyller, T. *Nat. Mater.* **2009**, *8*, 203−207.
(35) Sutter, P. W.; Flege, J.-I.; Sutter, E. A. *Nat. Mater.* **2008**, *7*, 406−411.
(36) Li, X.; Cai, W.; An, J.; Kim, S.; Nah, J.; Yang, D.; Piner, R.; Velamakanni, A.; Jung, I.; Tutuc, E.; Banerjee, S. K.; Colombo, L.; Ruoff, R. S. *Science* **2009**, *324*, 1312−1314.
(37) Cai, J.; Ruffieux, P.; Jaafar, R.; Bieri, M.; Braun, T.; Blankenburg, S.; Muoth, M.; Seitsonen, A. P.; Saleh, M.; Feng, X.; Muellen, K.; Fasel, R. *Nature* **2010**, *466*, 470−473.
(38) Li, D.; Mueller, M. B.; Gilje, S.; Kaner, R. B.; Wallace, G. G. *Nat. Nanotechnol.* **2008**, *3*, 101−105.
(39) Li, X.; Zhang, G.; Bai, X.; Sun, X.; Wang, X.; Wang, E.; Dai, H. *Nat. Nanotechnol.* **2008**, *3*, 538−542.
(40) Zhang, Z.; Xu, F.; Yang, W.; Guo, M.; Wang, X.; Zhanga, B.; Tang, J. *Chem. Commun.* **2011**, *47*, 6440−6442.
(41) Zhang, Z.; Chen, H.; Xing, C.; Guo, M.; Xu, F.; Wang, X.; Gruber, H. J.; Zhang, B.; Tang, J. *Nano Res.* **2011**, *4*, 599−611.
(42) Chen, X.; Wu, G.; Chen, J.; Chen, X.; Xie, Z.; Wang, X. *J. Am. Chem. Soc.* **2011**, *133*, 3693−3695.
(43) Yang, S.; Shen, C.; Liang, Y.; Tong, H.; He, W.; Shi, X.; Zhang, X.; Gao, H.-J. *Nanoscale* **2011**, *3*, 3277−3284.
(44) Zhang, Z.; Yang, W.; Zou, X.; Xu, F.; Wang, X.; Zhang, B.; Tang, J. *J. Colloid Interface Sci.* **2012**, *386*, 198−204.
(45) Deng, S.; Tjoa, V.; Fan, H. M.; Tan, H. R.; Sayle, D. C.; Olivo, M.; Mhaisalkar, S.; Wei, J.; Sow, C. H. *J. Am. Chem. Soc.* **2012**, *134*, 4905−4917.
(46) Lee, K. K.; Deng, S.; Fan, H. M.; Mhaisalkar, S.; Tan, H. R.; Tok, E. S.; Loh, K. P.; Chin, W. S.; Sow, C. H. *Nanoscale* **2012**, *4*, 2958−2961.
(47) Zhao, X.; Zhang, L.; Murali, S.; Stoller, M. D.; Zhang, Q.; Zhu, Y.; Ruoff, R. S. *ACS Nano* **2012**, *6*, 5404−5412.
(48) Sun, Y.; Hu, X.; Luo, W.; Huang, Y. *ACS Nano* **2011**, *5*, 7100−7107.
(49) Zou, Y.; Wang, Y. *Nanoscale* **2011**, *3*, 2615−2620.
(50) Ding, S.; Luan, D.; Boey, F. Y. C.; Chen, J. S.; Lou, X. W. *Chem. Commun.* **2011**, *47*, 7155−7157.
(51) Xu, J.; Wang, K.; Zu, S.-Z.; Han, B.-H.; Wei, Z. *ACS Nano* **2010**, *4*, 5019−5026.
(52) Vuluga, D.; Thomassin, J.-M.; Molenberg, I.; Huynen, I.; Gilbert, B.; Jerome, C.; Alexandre, M.; Detrembleur, C. *Chem. Commun.* **2011**, *47*, 2544−2546.
(53) Biswas, S.; Drzal, L. T. *Chem. Mater.* **2010**, *22*, 5667−5671.
(54) Liang, Y. Y.; Li, Y. G.; Wang, H. L.; Zhou, J. G.; Wang, J.; Regier, T.; Dai, H. J. *Nat. Mater.* **2011**, *10*, 780−786.
(55) Tao, L. Q.; Zai, J. T.; Wang, K. X.; Zhang, H. J.; Xu, M.; Shen, J.; Su, Y. Z.; Qian, X. F. *J. Power Sources* **2012**, *202*, 230−235.
(56) Yang, S. B.; Feng, X. L.; Ivanovici, S.; Mullen, K. *Angew. Chem., Int. Ed.* **2010**, *49*, 8408−8411.
(57) Gao, L. Z.; Zhuang, J.; Nie, L.; Zhang, J. B.; Zhang, Y.; Gu, N.; Wang, T. H.; Feng, J.; Yang, D. L.; Perrett, S.; Yan, X. *Nature Nanotechnol.* **2007**, *2*, 577−583.
(58) Mu, J. S.; Wang, Y.; Zhao, M.; Zhang, L. *Chem. Commun.* **2012**, *48*, 2540−2542.